Modeling of Multiconductor Buses and Analysis of Crosstalk, Propagation Delay, and Pulse Distortion in High-Speed GaAs Logic Circuits

GIOVANNI GHIONE, MEMBER, IEEE, IVAN MAIO, AND GIUSEPPE VECCHI

Abstract—**The paper presents an analysis of crosstalk, propagation delay, and pulse distortion in multiconductor buses for high-speed GaAs logic circuits. A simple but accurate quasi-TEM model of the bus is developed, and a critical analysis is carried out both on the accuracy of different approximate lumped and distributed models and on the impact of such approximations on the time-domain response. Results are presented on the behavior of multiconductor buses in the presence of realistic input waveforms, and design criteria are obtained.**

I. Introduction

THE BEHAVIOR of multiconductor interconnecting buses (MBUSes) is a critical issue in the design of large-scale and very large scale high-speed logic integrated circuits (IC's) on conventional or GaAs substrates. In fact, the performance improvements achieved through size reduction and use of new materials are partly lost after integration due to the *time delay* introduced by interconnections [1]. Moreover, circuit size reduction favors *crosstalk* in multiconductor buses, and frequency dispersive interconnections may cause strong *distortion* in short pulses.

The modeling of MBUSes has received considerable attention in the literature during the last few years. Although early works were based on *RC* models appropriate for low-speed IC's, buses for high-speed logics are usually modeled as multiconductor transmission lines. However, line characterization is often based on approximations valid for hybrid microstrip circuits, i.e., neglecting conductor losses [4], [6], [8], [18] and computing the parameters of the coupled lines according to simplified models [18]. Nonetheless, the models presented in [3], [5], [12], [13], and [17] include losses, and a recent paper [8] also presents results on dispersion. Concerning performance assessment, both time-domain [6], [16] and frequency-domain [18] techniques have been employed for transient analysis, and simplified CAD-oriented steady-state models for crosstalk evaluation have been presented in [4] and [9]. Finally, nonlinearity of loads and generators, which is neglected in this work, has been considered in [2] and [20].

Despite the fairly impressive amount of literature on MBUS characterization and transient analysis, some issues remain controversial. Since the frequency band whereon fast IC's operate can now extend well beyond 10 GHz, propagation effects are expected to take place in interconnections, thereby making *lumped* models possibly inadequate. Furthermore, the validity itself of transmission line models can be and has been questioned [21], since such models do not account for either free-space line or load radiation or surface-wave excitation. Nevertheless, if attention is restricted to coupling effects occurring *within* a loaded MBUS rather than *between* distant MBUSes, the quasi-TEM approach should be satisfactory, as discussed in Section II. On the other hand, typical MBUSes in high-speed IC's, whose strip width lies in the range 1–5 μm, have very high ohmic losses, which can make distributed lossless *LC* models less appropriate than lumped models including losses. Finally, owing to the reduction of rise times and pulse durations, and to the corresponding bandwidth enhancement, the design rules based on steady-state performance evaluation [4] become inadequate.

The aim of this paper is to develop a lossy quasi-TEM model for MBUSes on semi-insulating GaAs substrates and to simulate their transient response allowing for realistic termination of the connections, so as to correctly evaluate crosstalk, propagation delays, and pulse distortion. The analysis equally applies to Si substrates operating outside the slow-wave region. Particular stress is laid on a critical comparison with existing MBUS models. Approximations adequate for modeling coupled microstrips for analog applications or printed buses for low-speed logic circuits, such as neglecting conductor losses, evaluating the capacitance of the line by imposing cyclic boundary conditions [18], or neglecting the coupling between strips that are not neighboring (see e.g. [16]), are shown to be unsatisfactory in MBUSes for high-speed IC's. Finally, the impact of line

Manuscript received July 23, 1987; revised August 8, 1988.

G. Ghione is with the Department of Electronics, Politecnico di Milano, 20133 Milano, Italy.

I. Maio and G. Vecchi are with the Department of Electronics, Politecnico di Torino, 10129 Torino, Italy.

IEEE Log Number 8824624.

0018-9480/89/0300-0445$01.00

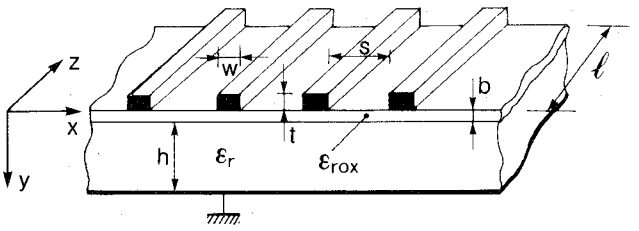

Fig. 1. Structure of the MBUS.

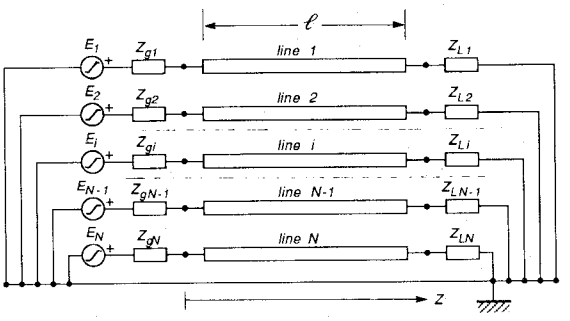

Fig. 2. Termination network for the MBUS.

modeling on transient simulation is investigated, and a discussion is presented on the validity of lumped models, with the aim of correcting some overly pessimistic remarks made on this point in [18].

The paper is structured as follows: after a statement of the problem, the quasi-TEM characterization of the structure is addressed, and the validity of several approximations proposed in the literature is discussed. Then, the transient problem is solved and design criteria are presented. Finally, the impact of different line models on transient results and the validity of lumped models are discussed.

II. Statement of the Problem

The high-speed VLSI bus considered is made of N parallel equispaced metallic strips deposited either on a semi-insulating layer (GaAs IC's) or on a thin oxide stratum supported by a semiconductor layer (Si IC's); a lower ground plane is also present (Fig. 1). Common values for N are powers of 2 (e.g. 8 or 16). The assumption of almost lossless substrate is well verified for GaAs substrates, but also for Si substrates if their conductivity and operation frequency are such as to avoid the onset of slow waves [10]. High losses occur in the conducting strips, whose width, thickness, and spacing usually fall into the range $w = 1$–10 μm, $t = 0.5$–2 μm, and $s = 1$–10 μm, respectively. (Note that typical values for microstrip lines in analog circuits are far larger, e.g. $w \approx 600$ μm, $t = 10$ μm for a thin-film 50 Ω line on 0.635-mm-thick allumina, and $w = 200$ μm for a 50 Ω line and $w = 80$ μm for a 70 Ω line on 0.3-mm-thick GaAs substrate.)

The structure is described with a quasi-TEM model, i.e., as a multiconductor transmission line characterized by a per-unit-length capacitance matrix $\underline{\underline{K}}$, inductance matrix $\underline{\underline{L}}$, resistance matrix $\underline{\underline{R}}$, and conductance matrix $\underline{\underline{G}}$, which can in principle depend on frequency. Since the substrate behavior is not dominated by dielectric losses, the conductance matrix will be neglected. The transmission line model implies a quasi-static treatment of the fields on the line cross section and does not account for radiation effects, which, however, are negligible when considering the interaction of conductors belonging to the *same* MBUS. In fact, as noticed in [21], static effects are dominant at *short* distances, such as those encountered *within* a bus. Conversely, crosstalk between *remote* buses, whose modeling is not addressed in this paper, is certainly affected by surface wave excitation; therefore, quasi-TEM models are expected to incorrectly estimate such interference. As a conclusion, we maintain that a transmission line model is meaningful in MBUS characterization as long as the interaction between *distant* structures is not investigated. The validity of the transmission line model is confirmed by its excellent agreement with measurements (see e.g. Fig. 7).

From the above discussion, we describe signal propagation on the bus through the well-known generalization of Kirchhoff equations (see e.g. [19]):

$$\frac{\partial \vec{v}(z,t)}{\partial z} = -\left(\underline{\underline{R}} + \underline{\underline{L}}\frac{\partial}{\partial t}\right)\vec{\imath}(z,t)$$
$$\frac{\partial \vec{\imath}(z,t)}{\partial z} = -\underline{\underline{K}}\frac{\partial}{\partial t}\vec{v}(z,t) \qquad (1)$$

where $\vec{v}(z,t)$, $\vec{\imath}(z,t)$ are the N-component current and voltage vectors. The bus is loaded (Fig. 2) on the right side by the input impedances of the next logic stage, and signals are fed from the left by voltage generators with proper internal impedance, simulating the output of the driving stage. The problem is now divided into two parts: determining the quasi-TEM parameters L_{ij}, K_{ij}, and R_{ij} of the MBUS and solving (1) with the boundary conditions imposed by generators and loads.

III. Multiconductor Bus Characterization

In this section a model for the quasi-TEM parameters of the MBUS is discussed. The adequacy of the model is investigated, and comparisons are carried out with previously presented models.

A. Evaluation of Capacitance and Inductance Matrices

The capacitance and inductance matrices of the MBUS can be evaluated by quasi-static techniques. In fact, although gigabit logics operate over a frequency range extending up to 20–30 GHz, the *frequency dispersion* typical of quasi-TEM modes is negligible, due to the reduced transversal dimensions of the structure. This conclusion is supported, e.g., by the full-wave analysis of a lossless multiconductor microstrip line carried out in [8] for a five-conductor MBUS much larger than a typical IC MBUS ($h = 1000$ μm against 300–400 μm; $w = 1000$ μm against 1–10 μm; $s = 200$ μm against 1–10 μm). By properly rescaling geometry and frequencies, mode dispersion appears to be negligible in integrated MBUSes at least up to 50 GHz. However, difficulties arise from the fact that conductors are *thick* and *penetrated by current*. The spec-

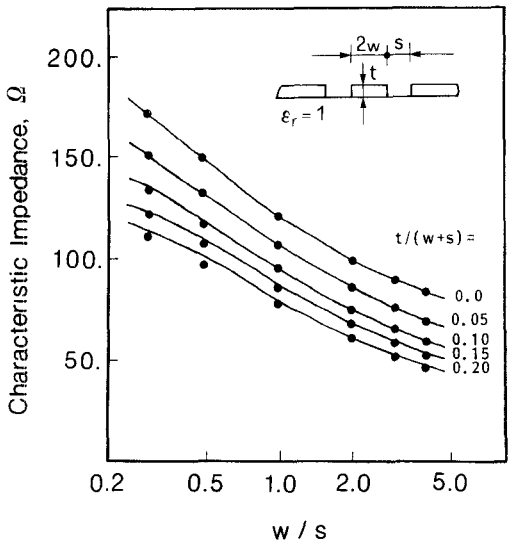

Fig. 3. Comparison between the characteristic impedances of thick perfectly conducting coplanar lines. Solid line: ref. [23]; dots: present approach.

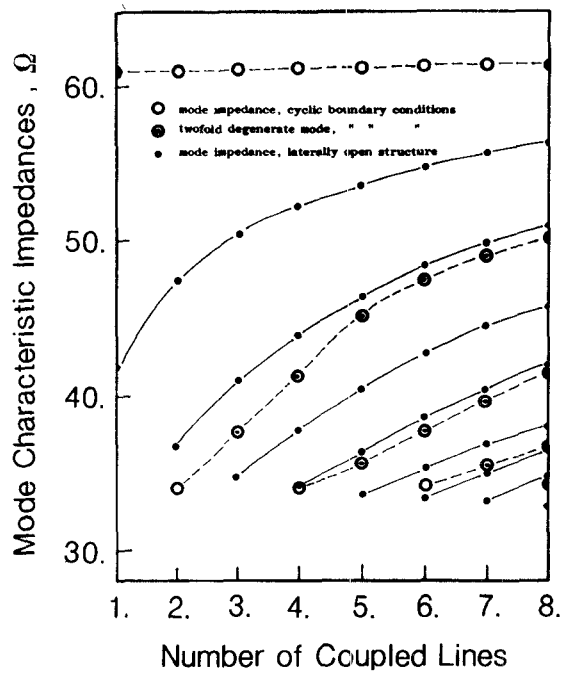

Fig. 4. Comparison between characteristic modal impedances for cyclic and open transversal boundary conditions as a function of line number. The (normalized) parameters are $w=1$, $t=0$, $s=1$, $h=1$, $b=0$, $\epsilon_r=12.9$, $\gamma=\infty$.

tral-domain Galerkin technique used here to evaluate the capacitance matrix (see the Appendix) allows such cases to be treated through a generalization of the perturbative approach proposed in [24]. In order to validate the model for the *thick strip* correction, a comparison has been carried out with the results reported in [23] for the impedance of a thick coplanar line (see Fig. 3); good agreement is found even for almost unit shape ratios. A coplanar structure has been chosen since the main contribution to the MBUS capacitance originates from coupling of coplanar neighboring strips rather than from coupling to ground. On the other hand, the amount of the correction due to considering a thick strip as *penetrated by current* is small even at low frequencies owing to the variational properties of the capacitance matrix with respect to the charge distribution. All computations presented have been carried out with surface charge density having proper edge singular behavior [11].

As is well known, the *inductance matrix* of perfectly conducting lines is proportional to the inverse of the capacitance matrix in air. In lossy lines, the total inductance matrix should also account for the internal (frequency-dependent) inductance of the strips, which can be evaluated for rectangular conductors as in [14, formulas (8) and (9)]. However, in the structures considered in this paper such contribution is usually small with respect to the external self-inductance. Therefore, we put $\underline{\underline{L}} \approx \frac{1}{c_0}\underline{\underline{K}}_0^{-1}$, where c_0 is the velocity of light in a vacuum and $\underline{\underline{K}}_0$ is the capacitance matrix in air. Comparisons with the data presented in [5] confirm the consistency of the approach.

Some comments on the model proposed in [18], and also adopted in [16], in which cyclic boundary conditions are imposed on the line cross section, are now in order. While such models offer computational advantages, results are in poor agreement with the laterally open model even in the presence of fairly low coupling between strips, as a comparison presented in Fig. 4 shows. (Note that the cyclic model admits pairs of degenerate modes having the same field topology and hence the same parameters.) In particular, if the overall width of the bus $W = N(w+s)-s$ is small in comparison with the substrate thickness, the impedance of the first even mode (also called *zero mode*, all strips at the same potential) takes on unphysically high values in the cyclic model (up to several kΩ, as already noted in [18], against the few hundred ohms found in the open structure). This discrepancy arises since imposing cyclic boundary conditions amounts, for the zero mode, to laterally shielding the bus with magnetic walls whose distance is $N(w+s)$. This way, the stray field of the line is suppressed, thereby leading to unphysically small capacitance when $W \ll h$. Finally, neglecting the coupling between nonneighboring lines, which leads to excellent results in microstrip couplers and printed circuit boards for low-speed applications [16], is unsatisfactory in MBUSes of small W/h ratio, as direct inspection of the capacitance matrix of such structures reveals.

B. Evaluation of Losses

In contrast to the use of *RC* models in characterizing interconnections for Si IC's, losses are neglected in most early works on MBUSes for fast logic circuits. However, *LC* models similar to those of coupled microstrip lines for microwave analog applications are invalid for lines having micronic width. Owing to the dramatic increase of conductor losses, the IC MBUSes considered here have complex characteristic impedance and very high attenuation over the whole operating frequency range and may show *RC* features up to several GHz.

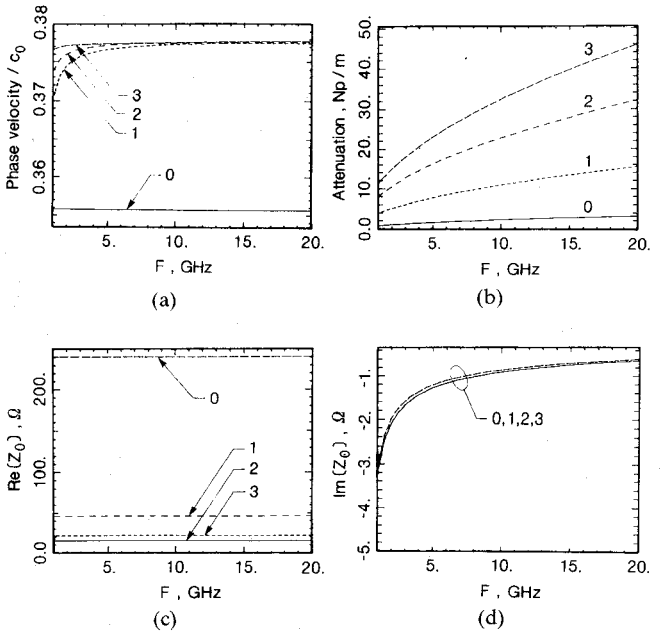

Fig. 5. (a) Normalized phase velocity; (b) attenuation (Np/m); (c) real and (d) imaginary part of characteristic impedances for a four-conductor MBUS with: $w = 30\ \mu$m, $s = 3\ \mu$m, $t = 3\ \mu$m, $h = 300\ \mu$m, $b = 0$, $\epsilon_r = 12.9$, $\gamma = 4 \cdot 10^7$ S/m. Curve labels refer to mode number (see text, subsection III-B).

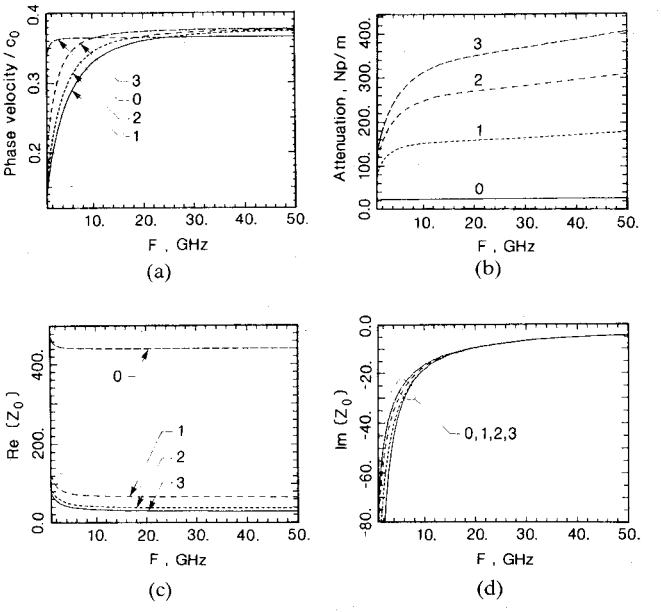

Fig. 6. (a) Normalized phase velocity; (b) attenuation (Np/m); (c) real and (d) imaginary part of characteristic impedances for a four-conductor MBUS with: $w = 2\ \mu$m, $s = 2\ \mu$m, $t = 0.6\ \mu$m, $h = 300\ \mu$m, $b = 0$, $\epsilon_r = 12.9$, $\gamma = 4 \cdot 10^7$ S/m. Curve labels refer to mode number (see text, subsection III-B).

As an example, let us consider the phase velocity, attenuation, and complex modal impedances (see subsection IV-A) of two four-conductor MBUSes. The first one has dimensions found e.g. in integrated Lange couplers, i.e., $w = 30\ \mu$m, $s = 3\ \mu$m, $t = 3\ \mu$m, $h = 300\ \mu$m; the second is an IC MBUS with $w = 2\ \mu$m, $s = 2\ \mu$m, $t = 0.6\ \mu$m, $h = 300\ \mu$m; the strip conductivity is $4 \cdot 10^7$ S/m. The results relative to the four propagation modes supported by the structure are shown in Figs. 5(a)–(d) and 6(a)–(d), respectively. In Figs. 5 and 6 mode 0 is the first even mode (i.e., the so-called zero mode, wherein all strips are at the same potential, see subsection IV-A), mode 1 is the first odd mode, and so forth. Even and odd modes are defined as in subsection IV-A. While the first bus behaves like an *LC* line with perturbative losses and almost real modal impedances already at 1 GHz, the second has dominant *RC* behavior up to 3–4 GHz and highly complex modal impedances up to about 15 GHz. Note that in multiconductor lines the effect of losses varies widely according to the propagation mode: the zero mode has high impedance and low losses, the other modes show lower impedance and higher losses due to proximity effects. Moreover, modes with dominant *RC* character can exist at a given frequency together with modes with dominant *LC* character. As a conclusion, not only is the lossless approximation inadequate for modeling high-speed MBUSes, but also the assumption that modal impedances are almost real is questionable in this case, while it holds in microstrip hybrid circuits.

Since conductors are completely penetrated by current over a considerable part of the operating frequency band [5], modeling of conductor losses according to skin-depth approximation is usually inappropriate. Taking into account that the distance between lines and the ground plane is large enough (with respect to the overall width of the bus) to allow both ground losses and the effect of the ground on the strip current distribution to be neglected [15], MBUS losses are characterized through the frequency-dependent resistance matrix of the strips. The resistance matrix is diagonal at zero frequency, and presents off-diagonal elements at higher frequencies due to coupling effects, which have been discussed in [5] and [6]. However, since such elements are subdominant up to millimeter-wave frequencies, we put $\{R_{ij}\} \approx \{R_i \delta_{ij}\}$, where R_i is the per-unit-length resistance of the strips ($R_i = R$ for identical strips), and δ_{ij} is the Kronecker delta.

Suitable approximations to the resistance of rectangular strips valid for the dc to skin-effect regime are presented in [14, formula 1]. Since lines have surface defects and irregularities (width variations of 0.2 μm on 1.5 μm strips are reported in [12] on a manufactured MBUS), which can be approximately accounted for through an average increase of resistivity [22], only a rough estimate of the effective conductivity γ is possible in the absence of measured data or detailed knowledge of the metallization process. Experimental data on lines with $w = 1.5\ \mu$m and 2.5 μm and typical thickness (approximately 0.5 μm) [12] yield dc resistances of 626 kΩ/m and 302 kΩ/m, respectively, corresponding to $\gamma = 2.1 \cdot 10^6$ S/m and $\gamma = 2.6 \cdot 10^6$ S/m, which agree with the values typical of composite metallization layers. As expected, lines with smaller cross section are more heavily affected by irregularities, and therefore have higher effective resistivity. In all the computations shown in the paper, metal conductivity was assumed to take on the average value $\gamma = 10^7$ S/m unless otherwise stated.

IV. Transient Behavior

A. Transient Analysis Technique

Since high-speed IC MBUSes behave as *RC* lines in the lower frequency range and as lossy *LC* lines above a critical frequency which depends on the propagation mode considered, the transient behavior changes according to the part of the frequency spectrum and the propagation modes that are actually excited. For low-speed signals the MBUS has mainly diffusive transients and strong signal distortion, whereas in the presence of higher speed signals propagation eventually dominates. Owing to the wide spectrum of the input signals, a *LC* model is never adequate, thereby preventing the application of time-domain transient techniques. Hence, transient simulation is performed by solving (1) through spectral-domain techniques, i.e., Fourier analysis and back-transformation. Since the procedure is standard, only a brief outline will be given.

First, the frequency-domain response of the lines (i.e., the spectra of the voltages and currents on the loads) is evaluated. According to standard multiconductor line analysis [19], we define the series impedance matrix as $\underline{\underline{Z}}_s = \underline{\underline{R}} + j\omega\underline{\underline{L}}$ and the parallel admittance matrix as $\underline{\underline{Y}}_p = j\omega\underline{\underline{K}}$. As is well known, a symmetrical grounded N-conductor line supports N propagation modes, which are classified as even or odd according to whether their potential distribution is even or odd with respect to the center of the line. Moreover, the mode index corresponds (in the lossless case) to the number of sign reversals occurring in the (modal) potential distribution. The N complex modal propagation constants $k_i = \beta_i - j\alpha_i$ (the forward wave amplitude is assumed to be proportional to $\exp(-jk_i z)$ and a time variation $\exp(j\omega t)$ is suppressed) will be a solution to the eigenvalue problem:

$$\left(k^2\underline{\underline{I}} + \underline{\underline{Z}}_s\underline{\underline{Y}}_p\right)\underline{\underline{M}}_u = 0$$

where $\underline{\underline{I}}$ is the identity matrix. $\underline{\underline{M}}_u$ is the *voltage eigenvector matrix*. The *current eigenvector matrix* $\underline{\underline{M}}_i$ can be obtained as

$$\underline{\underline{M}}_i = \omega\underline{\underline{K}}\underline{\underline{M}}_u \operatorname{diag}\{1/k_i\}$$

while the characteristic admittance matrix is found to be

$$\underline{\underline{Y}}_c = \underline{\underline{M}}_i\underline{\underline{M}}_u^{-1}.$$

The characteristic impedance matrix $\underline{\underline{Z}}_c$ is the inverse of $\underline{\underline{Y}}_c$, and the modal impedances are the eigenvalues of $\underline{\underline{Z}}_c$. Taking into account the definition of $\underline{\underline{M}}_u$, the voltage and current vectors on the lines can be written as

$$\begin{aligned}\vec{V}(z) &= \underline{\underline{M}}_u\left[\vec{W}^+(z) + \vec{W}^-(z)\right]\\ \vec{I}(z) &= \underline{\underline{Y}}_c\underline{\underline{M}}_u\left[\vec{W}^+(z) - \vec{W}^-(z)\right]\end{aligned} \tag{2}$$

where

$$\begin{aligned}\vec{W}^{\pm} &= \left\{W_i^{\pm}(z)\right\}\\ W_i^{\pm}(z) &= W_i^{\pm}(0)e^{\mp jk_i z}.\end{aligned} \tag{3}$$

W_i^+ and W_i^- are the amplitudes of the progressive and regressive components, respectively, of the ith mode, and k_i is the propagation constant of the ith mode. The arrays of generators and loads at the ends of the bus impose the following boundary conditions:

$$\begin{aligned}\vec{V}(0) &= \vec{E} - \underline{\underline{Z}}_g\vec{I}(0)\\ \vec{V}(l) &= \underline{\underline{Z}}_l\vec{I}(l)\end{aligned} \tag{4}$$

where $\vec{E} = \{E_i(\omega)\}$, $\underline{\underline{Z}}_g = \operatorname{diag}\{Z_{gi}\}$, and $\underline{\underline{Z}}_l = \operatorname{diag}\{Z_{li}\}$. E_i is the voltage spectrum of the generator at the input of the ith strip, Z_{gi} is the internal impedance of the ith generator, and Z_{li} is the impedance loading the ith strip.

On substituting (2) and (3) into (4) a linear system for $\vec{W}^{\pm}(l)$ is obtained:

$$\begin{pmatrix}\left(\underline{\underline{Y}}_l - \underline{\underline{Y}}_c\right)\underline{\underline{M}}_u & \left(\underline{\underline{Y}}_l + \underline{\underline{Y}}_c\right)\underline{\underline{M}}_u\\ \left(\underline{\underline{I}} + \underline{\underline{Z}}_g\underline{\underline{Y}}_c\right)\underline{\underline{M}}_u\underline{\underline{P}}^{-1} & \left(\underline{\underline{I}} - \underline{\underline{Z}}_g\underline{\underline{Y}}_c\right)\underline{\underline{M}}_u\underline{\underline{P}}\end{pmatrix}\begin{pmatrix}\vec{W}^+(l)\\ \vec{W}^-(l)\end{pmatrix} = \begin{pmatrix}\vec{0}\\ \vec{E}\end{pmatrix}, \qquad \underline{\underline{P}} = \operatorname{diag}\{e^{-jk_i l}\}. \tag{5}$$

Once (5) is solved, the voltage and current spectra can be obtained from (2). Finally, the time-domain response is obtained by Fourier transformation. All of the simulations presented were carried out through a standard FFT routine taken from the IMSL library. Since the analytical transform of typical input signals (e.g. voltage steps or square pulses) is available, only a frequency–time numerical transform is needed, thereby permitting easy monitoring of aliasing by direct inspection of the resulting time-domain waveforms. Problems were encountered with Gibbs's phenomenon while simulating lossless lines with low-resistance loads, since in this case the transfer function of the system does not provide enough filtering. Standard techniques, such as the use of Fejer kernels, have been adopted in this case.

In order to validate the model with experimental data, a comparison was performed on the transient behavior of single and coupled lines on GaAs substrates [12], [13]. The results are shown in Fig. 7 Despite the tolerance on the measured line dimensions (0.2 μm for w and s on lines with $w = 1.5$ μm, see [12, p. 133]) and the uncertainty on input and output resistances (see Fig. 7), estimated to be ± 20 percent [12], simulated results are in good agreement with measurements. Note that *LC* parameters were computed from the geometry, whereas the metallization resistivity was fitted on the measured dc line resistance.

B. Interpretation of Transient Behavior and Design Considerations

In order to highlight the features of the transient response of the MBUS, it is useful to discuss an idealized case in which the problem can be solved explicitly. Namely, if we consider a lossless MBUS with cyclic boundary conditions and if $Z_{li} = Z_l$, $Z_{gi} = Z_g$, and $E_i = E\delta_{ik}$ (all load and generator impedances are equal and the signal is

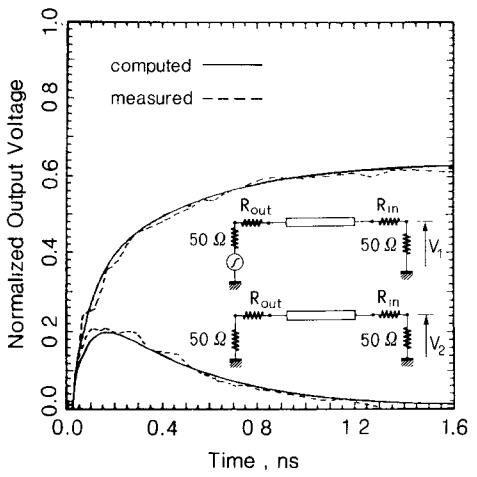

Fig. 7. Comparison between numerical and measured results for two coupled lines. Solid line: numerical simulation; dashed line: experimental results [12], [13]. Excitation with a tapered unit step with t_{rise} = 40 ps, $w = 1.5\ \mu$m, $s = 2\ \mu$m, $t = 0.5\ \mu$m, $h = 400\ \mu$m, $b = 0$, $\epsilon_r = 12.8$, $\gamma = 2.1 \cdot 10^6$ S/m, $l = 3$ mm, $R_{in} = 2100\ \Omega$, $R_{out} = 380\ \Omega$.

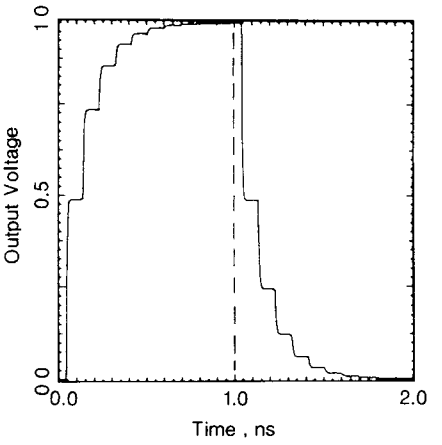

Fig. 8. Typical modal line contribution (lossless case). Solid line: output voltage of zeroth mode of the IC-MBUS of Fig 9. Dashed line: input signal, 1 ns unit square pulse. Characteristic impedance is $Z = 166.422\ \Omega$, normalized phase velocity is $v/c_0 = 0.384$. The reflection coefficient is $\rho = 0.51$ (see formula (7))

fed into line k only), system (5) admits the following solution:

$$\begin{cases} V_l(\omega) = \left\{ \dfrac{1}{N} \displaystyle\sum_{n=0}^{N-1} \exp\left(j\frac{2\pi}{N} n(i-k) \right) g_n(\omega) \right\} E(\omega) \\ g_n(\omega) = \dfrac{(1-\rho_n)(1+\Gamma_n(\omega)) e^{-jk_n l}}{2(1-\rho_n \Gamma_n(\omega) e^{-jk_n 2l})} \end{cases} \tag{6}$$

where ρ_n, Γ_n are the reflection coefficients of Z_g, Z_l with respect to the characteristic impedance of the nth mode, Z_n. Since the functions $g_n(\omega)$ are simply the transfer functions of a loaded LC line, formula (6) describes the output voltage spectra as a superposition of N modal line contributions. Back-transformation to the time domain yields

$$v_l(t) = \frac{1}{N} \left\{ \sum_{n=0}^{N-1} \exp\left(j\frac{2\pi}{N} n(i-k) \right) h_n(t) \right\} \tag{7a}$$

where $h_n(t)$ is the inverse Fourier transform of $g_n(\omega)E(\omega)$. Let us suppose now that the load is capacitive (C_{load}) and the generator impedance is resistive (R_{gen}). In this practically important case, the modal line contribution $h_n(t)$ can be expressed through a multiple reflection expansion, which, when the driving voltage is a unit step, reads,

$$h_n(t) = (1-\rho_n) \sum_{m=0}^{\infty} \rho_n^m \left(1 - \Phi_m^{(n)}\left(\tau_m^{(n)}\right)\right) u\left(\tau_m^{(n)}\right)$$

$$\tau_m^{(n)} = t - (2m+1)T_n \qquad T_n = l/v_n \qquad a_n = 1/C_{load} Z_n$$

$$\Phi_m^{(n)}(\tau) = e^{-a_n \tau} \sum_{k=0}^{m} \binom{m}{k} (-1)^{m-k} 2^k \sum_{i=0}^{k} \frac{(a_n \tau)^i}{i!} \tag{7b}$$

where $u(t)$ is the unit step function. The quantity $h_n(t)$ exhibits a well-known staircase shape, which results from a superposition of echoes (see Fig. 8). Since the mth echo is zero for $t < (2m+1)T$ and tends to $(1-\rho)\rho^m$ for $t \to \infty$ (if $\rho < 1$), the step width is T and the step height decreases with increasing echo order. From (7a) the output voltage on each line is a superposition of staircase waveforms. For $t \to \infty$ a constant value results, which is *zero* for the nonenergized lines, as can easily be seen on applying the final value theorem to (6).

The above remarks are still able to provide insight into the shape of the voltage responses of *realistic* MBUSes to typical digital input signals. Two examples of response are given in Figs. 9(a), 10(a) (line losses are neglected) and in Figs. 9(b), 10(b) (line losses included). These waveforms can still be interpreted as a superposition of curves of the kind shown in Fig. 8, each one characterized by the transit time and generator mismatch of one of the modes, although the restrictions leading to the analytical solution (7a) and (7b) have been waived. Notice that metallization losses can be, at least approximately, assimilated to an increase of the resistance loading the circuit. As a conclusion, the matching of the generator resistance to the line impedance and the modal transit times T_n can be considered as the factors which determine the shape of the transient waveforms also in realistic MBUSes.

Since *signal distortion* on the driven line is mainly due to the staircase profile of the waveform, impedance matching with generators is the most effective way of reducing distortion in a MBUS of a given length. As *time delay* depends both on the transit time and on the rise time of the waveform, this parameter too is optimized, for a given structure, through impedance matching with the output of the driving stage. A further contribution to signal distortion comes from phase velocity mismatch between modes, owing to which modal echoes have different arrival times. However, phase velocity equalization has a positive influence only in the presence of good impedance matching,

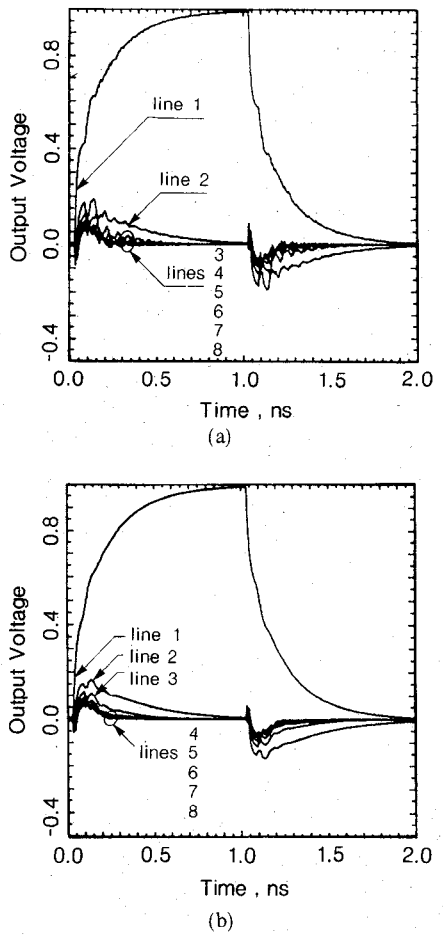

Fig. 9. Response of eight-conductor IC MBUS to a unit 1 ns voltage pulse applied to line 4. (a) Lossless case. (b) With lossy strips of conductivity $\gamma = 4 \cdot 10^7$ S/m. The parameters are $w = 3$ μm, $t = 0.5$ μm, $s = 4$ μm, $h = 400$ μm, $l = 5$ mm, $b = 0$, $\epsilon_r = 12.9$; terminations, $R_g = 500$ Ω, $C_l = 20$ fF on all lines.

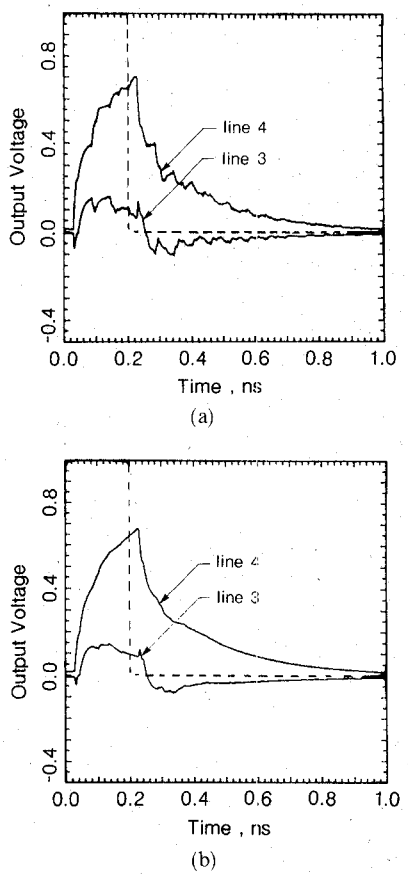

Fig. 10. Response of the same structure as in Fig. 9 to typical high-speed digital signals: 0.2 ns square pulse applied to line 4. (a) Lossless and (b) lossy strips of conductivity $\gamma = 4 \cdot 10^7$ S/m. Only the responses of lines 4 and 3 are shown.

since only in this case is the overall rise time of the line actually reduced. Finally, typical structures do not present strong *intersymbolic interference* unless high mismatch with the generator occurs (see e.g. Fig. 10).

Concerning *crosstalk*, we consider only the so-called far-end crosstalk (i.e., the voltage induced on the *load* of a nonenergized line) as opposed to near-end crosstalk (i.e., the voltage induced on the *input* of a nonenergized line). Moreover, we define crosstalk as a peak voltage ratio rather than with reference to the energy of the coupled disturbance; the two values, however, do not appreciably differ in ordinary load conditions. Standard steady-state evaluation of coupling, as has been already noted [18], fails to bring out accurate information on crosstalk, unless very simple lumped equivalent circuits of the MBUS are assumed to be valid. For instance, if a capacitively loaded "lumped capacitance" model is considered (see the discussion in [18, appendix]) and only one line is fed by an ideal voltage generator while the remaining lines are open-circuited, far-end crosstalk and near-end crosstalk coincide and the waveforms on both the energized line (i) and the inactive ones (j) are proportional through a factor P_{ij}/P_{ii}, where $\{P_{ij}\}$ is the elastance matrix of the (loaded) capacitive lumped equivalent circuit [4], [9]. The corresponding crosstalk values are usually *higher* than those foreseen by a distributed model. Apart from yielding a rule-of-thumb conservative design rule, the steady-state model is basically incorrect since it does not account for the fact that crosstalk also depends on the *time derivatives* of the driving signal, as can be seen from the frequency-domain solution (eqs. (6) and (7)).

Conversely, capacitive lumped models, but with realistic generator loadings, tend to *underestimate* peak crosstalk when the circuit actually shows high-Q resonances, since they have RC (diffusive) transients. High-Q ringings appear in the response when the MBUS has high distributed inductance, is capacitively loaded, and the internal resistance of generators is low (e.g. under 100 Ω). This case is discussed in detail in [18]; however, we point out that, at least for GaAs logics and considering a correct LC model of the MBUS including losses, such strongly resonant behavior is hardly ever found. This point will be discussed in more detail in the next section.

Transient simulation of crosstalk yields results in agreement with the qualitative discussion presented. First, the peak amplitude of crosstalk is very sensitive to variations in *pulse rise time* on the driving line. However, when the pulse rise time becomes much lower than the dominant time constant of the circuit, no further increase results

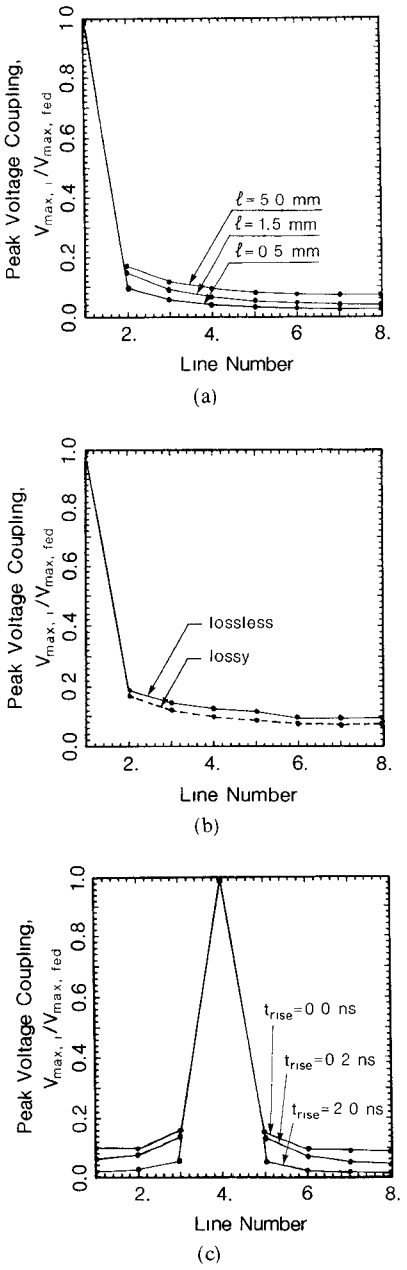

Fig. 11. Peak voltage coupling for the IC-MBUS of Fig. 9. (a) Effect of interconnection length l, lossless, and (b) effect of lossy lines, l = 5 mm; the input signal is a square pulse of rise time 0.2 ns. (c) Effect of rise time, lossy line.

since the high-frequency tail of the input spectrum is filtered out. This suggests pessimistic considerations on the impact of crosstalk in superconductive logic circuits. If the resistive component of the circuit is drastically reduced and logic gate speed is increased, peak crosstalk is bound to increase beyond the values which are encountered in ordinary circuits. *Interconnection length* appears to play a lesser role on crosstalk amplitude, which is slightly greater for long MBUSes than for short ones, if conductor losses are neglected. If conductor losses are included in the model, no appreciable difference can be detected in far-end crosstalk beyond a certain length (typically a few mm). *Losses* tend to reduce crosstalk owing to their damping effect, and so does an increase of the generator resistance. This last effect was examined in detail in [18]; note that in GaAs logics the generator resistance is comparatively high (a few hundred ohms). These remarks are supported by the results shown in Fig. 11(a)–(c), where the influences on crosstalk of interconnection length, metallization losses, and driving pulse rise time, respectively, are highlighted. The well-known dependence of crosstalk on the distance between neighboring strips needs no further comment.

C. Impact of Line Characterization on Transient Behavior

In the present section the influence of line characterization on the simulated transient response of the MBUS is discussed. Since the MBUS is characterized in the frequency domain such an influence cannot be easily appreciated *a priori*; in other words, characterizations being inaccurate over part of the operating bandwidth (e.g. lossless ones) can lead to fairly acceptable transient results in the presence of proper input signals.

Let us first consider the effect of losses on the frequency-domain transfer function of the MBUS. As an example, we will consider the transfer function of a single (modal) line; the load is capacitive and the generator impedance is resistive. The introduction of losses (see Fig. 12(a) and (b)) amounts to a damping effect on the resonances of the transfer function of the line; i.e. the lossier the line, the deeper the resonant poles of the transfer function are pushed into the complex plane. Such an effect is hardly noticeable in typical microstrip lines for analog microwave applications, since in this case losses are dominated by the load resistance (Fig. 12(b), continuous and dashed lines), whereas it can be considerable in micronic microstrip lines (Fig. 12(a)). Since an increase of losses leads to a greater damping of the high-frequency component of the spectrum, it is clear how a concentrated model for the line (which does not reproduce the upper part of the spectrum of the distributed line response) yields better results for high-loss structures than for low-loss analog lines. These remarks are supported by the results shown in Fig. 12(a) and (b) (dashed-dotted lines), where the transfer functions of a concentrated (single-cell) model of the line are presented for the two cases mentioned above.

Such an interpretation is confirmed when considering the effect of losses on the time-domain response of the MBUS. As an example, the transient behavior of an eight-conductor MBUS 5 mm long is shown in Figs. 9 and 10 for the two cases where losses are neglected (Figs. 9(a), 10(a)) or included (Figs. 9(b), 10(b)); the input signal is a square pulse with zero rise time. From these results, losses have two main effects on the output pulse shape: first, the staircase rising profile of the waveform is smeared out with respect to the lossless case; second, the output voltages on the secondary lines show lower amplitude ringings when compared to the lossless case, meaning lower crosstalk between lines. A further, less important effect is the increased rise time on the energized line, caused by the increased overall resistance of the circuit. This effect, which

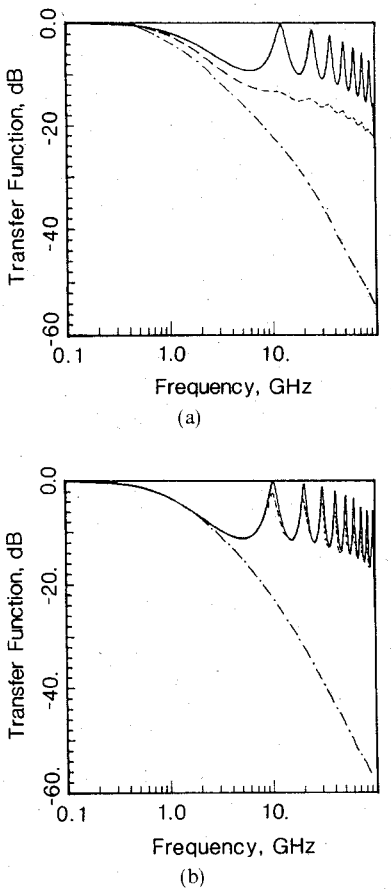

Fig. 12. Comparison between single-line frequency-domain transfer function for: (a) Typical IC-MBUS strip, parameters as in Fig. 9. Solid line: lossless ($\gamma = \infty$); dashed line: lossy strip $\gamma = 1 \cdot 10^7$ S/m; dashed–dotted: single-cell lumped model (lossy strip). (b) Typical analog microstrip line; $w = 80$ μm, $t = 7$ μm, $h = 300$ μm, $b = 0$ μm, $\epsilon_r = 12.9$. Solid line: lossless ($\gamma = \infty$), dashed line: lossy strip, $\gamma = 1 \cdot 10^6$ S/m, dashed–dotted: single-cell lumped model (lossy strip). Terminations are $R_g = 250$ Ω, $C_l = 20$ fF.

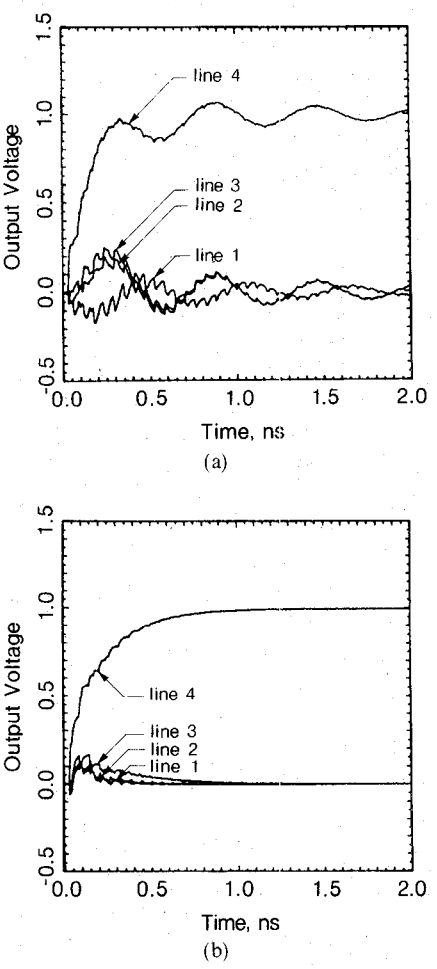

Fig. 13. Comparison between step response for the IC-MBUS of Fig. 9 with (a) cyclic and (b) open transversal boundary conditions. The MBUS is considered lossless, and only the responses of lines 1,2,3,4 are shown.

is not appreciable in the example shown, could also be simulated by adding to the load or generator impedances the total resistance of the line and by treating the line as lossless (see the example in [5] and compare with [6]). This approximation, however, is inaccurate whenever truly distributed *RC* effects are important; in particular, it does not account for the influence of losses on phase velocity.

Concerning *LC* characterization, let us consider the impact of the *cyclic* model on transient simulation. A comparison between the transient responses of a lossless eight-conductor MBUS to a voltage step is shown in Fig. 13, with cyclic (Fig. 13(a)) and exact (Fig. 13(b)) transversal boundary conditions. The main differences between the two responses are that 1) the cyclic line shows voltage overshoot, whereas the ordinary one does not and 2) the cyclic line has greater crosstalk and pulse distortion. Such discrepancies can be explained with reference to formulas (6) and (7) and the related discussion. Since, as already noted, the even-mode line impedance takes on an unphysically high value in the cyclic model, the reflection coefficient relative to this mode has almost unit value when typical generator impedances are considered. Hence, the poles of the transfer function (6) relative to the zero mode line are almost real and represent high-Q resonances which dominate the overall response of the MBUS. As a conclusion, the cyclic boundary condition technique does not lead to a correct estimate of the line response for the typical dimensions encountered in MMIC buses, while good results are obtained for loosely coupled structures (see e.g. [16]).

D. Validity of Lumped Models

CAD-oriented lumped models of MBUSes are still popular owing to their simple implementation in time-domain analysis codes, such as SPICE. Most lumped models consist of *RC* cells, and neglect conductor inductance [1].

As an obvious rule, lumped models yield accurate results whenever the multiconductor line is "short" in terms of the operating wavelength over the whole frequency band of interest. Therefore, not only the line length l but also the input signal dictates whether the lumped model is appropriate. If single-cell *RLC* models provide no information on signal delay, such models actually yield fairly accurate results for both rise time and crosstalk when the MBUS is short. In Fig. 14 we show the response of a

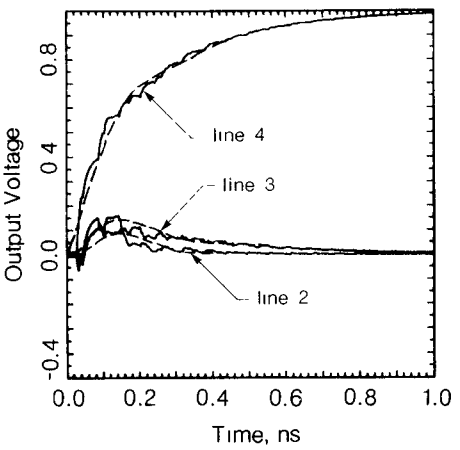

Fig. 14. Comparison between step response with lossless distributed (solid line) and LC lumped model (dashed line). Same IC-MBUS as in Fig. 9. Only the responses of lines 2,3,4 are shown.

lossless eight-conductor MBUS ($l = 5$ mm) to a voltage step, computed either by means of a distributed model (continuous line) or a lumped model (dashed line). The per-unit-length line parameters are the same in both cases, and the lumped model is a single cell consisting of a series impedance matrix and a parallel admittance matrix of values $Z_s l$ and $Y_p l$, respectively. Apart from the initial delay of the rising front, the two models yield similar results in both pulse energy and crosstalk, although the response of the lumped model on the secondary lines does not show any ringings caused by echoes; even better agreement is found when losses are considered. Further results (not shown here for the sake of brevity) bring out that lumped models where inductance is neglected do not lead to completely meaningless results unless for very short pulses, but tend to significantly underestimate crosstalk. These results suggest that the pessimistic comments on the validity of lumped models reported in [18] should be handled with some care. In fact, such comments are supported by a comparison between the response of a MBUS characterized by the cyclic model (having high even-mode inductance per unit length) and the response of a lumped model, wherein *the inductance is neglected*. As a consequence, large but unphysical discrepancies arise between the two responses.

As a conclusion, we suggest that for short lines, and when signal delay is not relevant, lumped models are actually able to yield fairly accurate estimates of crosstalk, whereas owing to the absence of the echoes which characterize the distributed model, the actual pulse shape is only approximately reproduced. As a rule of thumb, the maximum line length for which a lumped model is expected to hold can be estimated, for a square input pulse of width τ whose spectrum is truncated to the $(n+1)$th zero, as

$$l_{\max} = \tau c_0 / \left(16 n \sqrt{\epsilon_{\text{eff}}}\right)$$

where c_0 is the velocity of light in a vacuum. The maximum length is chosen as the one leading to a phase error of $\pi/4$ at the maximum frequency considered, and the effective permittivity ϵ_{eff} is taken as an average value on the line modes. For instance, with a pulse width of 0.5 ns, $n = 1$, one has $l_{\max} = 3.54$ mm.

V. Conclusions

An analysis of crosstalk, propagation delay, and pulse distortion on multiconductor buses for high-speed GaAs logic circuits has been developed. The analysis is based on a simple but accurate quasi-TEM multiconductor transmission line model which includes losses and makes no significant approximations in evaluating the line parameters. The model has been validated through comparison with available experimental results. Our results can be summarized as follows:

- Lossless (LC) models, which yield accurate results in ordinary microstrip lines for microwave analog applications, are inadequate for evaluating crosstalk, pulse distortion, and pulse rise time in VLSI MBUSes. In particular, LC models overestimate crosstalk and pulse distortion and slightly underestimate the overall pulse rise time.
- Models assuming cyclic boundary conditions on the device cross section lead to substantial errors in evaluating the line parameters of realistic structures.
- Lumped models are fairly accurate in modeling short multiconductor buses provided that the model is complete (i.e., includes not only capacitive coupling and resistive elements, but also inductive coupling) and its parameters are evaluated correctly. Since multiconductor buses in high-speed IC's are often electrically short, simple lumped models should be suitable in many conditions, thereby avoiding the need to resort to distributed models which are often difficult to implement and time-consuming in standard circuit analysis codes (e.g. SPICE).
- The role of generator mismatch on pulse distortion has been assessed: the higher the mismatch, the greater the pulse distortion. Crosstalk has been shown to depend only weakly on the multiconductor bus length but to be heavily increased by pulse rise time reduction.

Appendix
Spectral-Domain Evaluation of the Capacitance Matrix

Let us consider a multiconductor line on a layered dielectric substrate; for the moment, metallic strips are supposed to have zero thickness. Let $\phi(x)$ be the potential and $\rho(x)$ the charge density on the interface whereon the strips are located. The Fourier transforms $\Phi(k_x)$, $P(k_x)$, defined as

$$\Phi(k_x) = \int_{-\infty}^{+\infty} \phi(x) e^{-jk_x x}\, dx \tag{A1}$$

and similarly for $P(k_x)$, are related as follows:

$$\Phi(k_x) = \frac{1}{\epsilon_0} G(k_x) P(k_x) \tag{A2}$$

where ϵ_0 is the vacuum permittivity, and the spectral-domain static Green's function $G(k_x)$ can be computed as in [7]. The functional equation (A2) can be solved by the spectral-domain Galerkin method. Let us approximate the charge density as

$$\rho(x) = \sum_j Q_j^{(n)} r_j^{(n)}(x) \tag{A3}$$

where the superscript (n) refers to the nth strip, $r_j^{(n)}(x)$ is a set of basis functions satisfying the boundary conditions on the strips, and $Q_j^{(n)}$ are weights to be determined. The potential on the interface can be decomposed as follows:

$$\phi(x) = \phi_1(x) + \sum_n V^{(n)} p^{(n)}(x) \tag{A4}$$

where $\phi_1(x)$ is the (unknown) potential between strips, $V^{(n)}$ the potential on the nth strip, and $p^{(n)}(x)$ is 1 on the nth strip and 0 outside. Finally, let us define the total charge on the nth strip as

$$Q^{(n)} = \sum_{j(n)} Q_j^{(n)} q_j^{(n)} \tag{A5}$$

where $j(n)$ means that the summation on j is extended to all basis functions relative to the nth strip, and

$$q_j^{(n)} = \int_{\substack{n\text{th} \\ \text{strip}}} r_j^{(n)}(x)\, dx. \tag{A6}$$

If the Fourier transform of (A3) is substituted into (A2) and the equation thereby obtained is multiplied by $R_i^{(m)*}(k_x)$ (i.e., by the conjugate of the Fourier transform of the trial charge distribution $r_i^{(m)}(x)$) and integrated on the whole spectral domain, one obtains

$$\int_{-\infty}^{+\infty} R_i^{(m)*}(k_x)\Phi(k_x)\, dk_x = \sum_j Q_j^{(n)} \int_{-\infty}^{+\infty} R_i^{(m)*}(k_x) G(k_x) R_j^{(n)}(k_x)\, dk_x. \tag{A7}$$

On applying Parseval's theorem to the left-hand side and taking into account (A3), (A4), and (A6) one can write (A7) in the form

$$V^{(m)} q_i^{(m)} = \sum_j E_{ij} Q_j^{(n)} \tag{A8}$$

where

$$E_{ij} = \frac{1}{2\pi} \int_{-\infty}^{+\infty} R_j^{(n)}(k_x) G(k_x) R_i^{(m)*}(k_x)\, dk_x. \tag{A9}$$

If we define $\{C_{ij}\}$ as the inverse of $\{E_{ij}\}$, we have

$$Q_i^{(m)} = \sum_j C_{ij} q_j^{(n)} V^{(n)} = \sum_n \sum_{j(n)} C_{ij} q_j^{(n)} V^{(n)} \tag{A10}$$

and, finally, taking into account (A5),

$$Q^{(m)} = \sum_n K_{mn} V^{(n)} \tag{A11}$$

where the capacitance matrix element is expressed as

$$K_{mn} = \sum_{i(m)} \sum_{j(n)} q_i^{(m)} C_{ij} q_j^{(n)}. \tag{A12}$$

In order to account for thick strips penetrated by current, an extension of the approach followed in [24] is proposed. By approximating the charge profile *across* the strip as in an infinitely wide strip, a spectral-domain approximate integral equation is obtained on imposing constant potential on the strip bases (rather than on the whole strip contour). One again obtains (A2), but the Green's function is multiplied by the factor

$$F(k_x) = \frac{1 + e^{-k_x t}}{2(1 - k_x^2 \delta^2)} \left[1 - k_x \delta \tanh\left(\frac{k_x t}{2}\right) \coth\left(\frac{t}{2\delta}\right) \right] \tag{A13}$$

where δ is the skin penetration depth and t is the strip thickness. For $\delta \to 0$ the correcting factor proposed in [24] is obtained. Note that (A13) holds whenever the line is not covered. While the correction due to finite strip thickness is significant, the final result depends only weakly on δ.

ACKNOWLEDGMENT

The authors wish to thank Prof. J. Citerne (I.N.S.A., Rennes, France) for kindly providing a copy of the doctorate thesis [12]. Helpful discussions with Prof. F. Gregoretti of the Dipartimento di Elettronica, Politecnico di Torino, are also gratefully acknowledged.

REFERENCES

[1] M. Annaratone, *Digital CMOS Circuit Design*. Boston: Kluwer Academic Publishers, 1986, ch. 5.

[2] S. P. Castillo, C. H. Chan, and R. Mittra, "Analysis of N-conductor transmission line systems with non-linear loads with application to CAD design of digital circuits," in *Proc. 1986 Int. Symp. Electromagn. Compat.*, Sept. 1986, pp. 174–175.

[3] J. Chilo, G. Angenieux, and C. Monnlor, "Proximity effects of interconnection lines in high-speed integrated logic circuits," in *Proc. 13th European Microwave Conf.*, 1983, pp. 369–373.

[4] J. Chilo, G. Angenieux, and T. Razban, "CAD formulas for modelling the interconnections of fast GaAs integrated circuits," in *Proc. 15th European Microwave Conf.*, 1985, pp. 509–514.

[5] J. Chilo, C. Monnlor, and M. Bouthinon, "Interconnection effects in fast logic integrated GaAs circuits", *Int. J. Electron.*, vol. 58, no. 4, pp. 671–686, 1985.

[6] J. Chilo and T. Arnaud, "Coupling effects in the time domain for an interconnecting bus in high-speed GaAs logic circuits," *IEEE Trans. Electron Devices*, vol. ED-31, pp. 347–352, Mar. 1984.

[7] R. Crampagne, M. Ahmadpanah, and J L. Guiraud, "A simple method for determining the Green's function for a large class of MIC lines having multilayered dielectric structures," *IEEE Trans. Microwave Theory Tech.*, vol. MTT-26, pp. 82–87, Feb. 1978.

[8] E. G. Farr, C. H. Chan, and R. Mittra, "A frequency-dependent coupled-mode analysis of multiconductor microstrip lines with application to VLSI interconnection problems," *IEEE Trans. Microwave Theory Tech.*, vol. MTT-34, pp. 307–310, Feb. 1986.

[9] G. Ghione and C. Naldi, "Analysis of crosstalk on multiconductor buses in high-speed GaAs integrated circuits: A statistical approach," in *Proc. 1987 Int. Microwave Symp.* (Rio de Janeiro), July 1987, pp. 95–100.

[10] H. Hasegawa, M. Furukawa, and H. Yanai, "Properties of microstrip line on Si–SiO_2 system," *IEEE Trans. Microwave Theory Tech.*, vol. MTT-19, pp. 869–881, Nov. 1971.

[11] R. Mittra and S. W. Lee, *Analytical Techniques in the Theory of Guided Waves*. New York: MacMillan, 1971.

[12] N. Moisan, "Etude théorique et expérimentale des effets de propagation dans les circuits logiques rapides," Doctorate thesis, Institut National des Sciences Appliquées de Rennes, France, Oct. 1986.

[13] N. Moisan, J. M. Floc'h and J. Citerne, "Efficient modelling technique of lossy microstrip line sections in digital GaAs circuits," in *Proc. 16th European Microwave Conf.*, 1986, pp. 698–704.

[14] E. Pettenpaul *et al.*, "CAD models of lumped elements on GaAs up to 18 GHz," *IEEE Trans. Microwave Theory Tech.*, vol. MTT-36, pp. 294–304, Feb. 1988.

[15] V. Rizzoli, "Losses in microstrip arrays," *Alta Frequenz*, vol. XLIV, no. 2, pp. 86–94, 1975.

[16] F. Romeo and M. Santomauro, "Time-domain simulation of n coupled transmission lines," *IEEE Trans. Microwave Theory Tech.*, vol MTT-35, pp. 131–137, Feb. 1987.

[17] C. Seguinot, P. Kennis, P. Pribetich, and J. F. Legier, "Crosstalk phenomenon in coupled microstrip lines laid on semi-conducting substrates," in *Proc. 15th European Microwave Conf.*, 1985, pp. 826–830.

[18] S. Seki and H. Hasegawa, "Analysis of crosstalk in very high-speed LSI/VLSI's using a coupled multiconductor MIS microstrip line model," *IEEE Trans. Microwave Theory Tech.*, vol. MTT-34, pp. 1715–1720, Dec. 1986.

[19] J. Siegl, V. Tulaja, and R. Hoffmann, "General analysis of interdigitated microstrip couplers," *Siemens Forsch.-u. Entwickl.-Ber.*, vol. 10, no. 4, pp. 228–236, 1981.

[20] T. K. Sarkar, A. R. Djordjevic, and R. F. Harrington, "Analysis of lossy transmission lines with arbitrary nonlinear terminal networks," *IEEE Trans. Microwave Theory Tech.*, vol. MTT-34, pp. 660–666, June 1986.

[21] T. K. Sarkar and J. R. Mosig, "Comparison of quasi-static and exact electromagnetic fields from a horizontal electric dipole above a lossy dielectric backed by an imperfect ground plane," *IEEE Trans. Microwave Theory Tech.*, vol. MTT-34, pp. 379–387, April 1986.

[22] H. Sobol, "Application of integrated circuit technology to microwave frequencies," *Proc. IEEE*, vol. 59, pp. 1200–1211, Aug. 1971.

[23] E. Shu, K. Koshiji, and S. Michi, "Simplified computation of coplanar waveguide with finite conductor thickness," *Proc. Inst. Elec. Eng.*, vol. 130, pt. H, no. 5, pp. 315–321, Aug. 1983.

[24] E. Yamashita, "Variational method for the analysis of microstrip-like transmission lines," *IEEE Trans. Microwave Theory Tech.*, vol. MTT-16, pp. 529–535, Aug. 1968.

✠

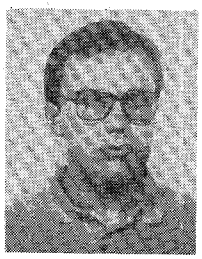

Giovanni Ghione (M'87) received the Laurea degree in electronic engineering from the Politecnico di Torino, Torino, Italy, in 1981. From 1983 to 1987 he was with the Department of Electronics at the Politecnico di Torino as a researcher; in 1987 he joined the Politecnico di Milano as an Associate Professor. His current research activities concern the modeling of passive and active components for MMIC's (coplanar and multiconductor lines, two-dimensional physical modeling of MESFET devices) and low- and high-frequency electromagnetics.

Mr. Ghione is a member of AEI (Associazione Elettrotecnica Italiana).

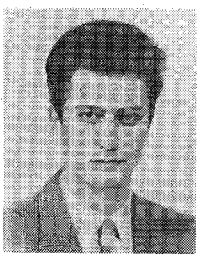

Ivan Maio received the Laurea degree in electrical engineering from the Politecnico di Torino, Torino, Italy, in 1986. Currently, he is working toward the Ph.D. degree at the Politecnico di Torino. His research interests have focused mainly on nonlinear optics, coherent optical communication, and semiconductor lasers.

✠

Giuseppe Vecchi received the Laurea degree in electronic engineering from the Politecnico di Torino, Torino, Italy, in 1985. He worked as a technical consultant until January 1987, when he entered the Ph.D. program in electronic engineering at the Politecnico di Torino. His main research interests are in frequency- and time-domain propagation and scattering from complicated structures.